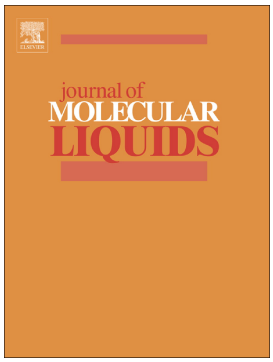


# Ionic liquid crystals: Synthesis and characterization via NMR, DSC, POM, X-ray diffraction and ionic conductivity of asymmetric viologen bistriflimide salts

Pradip K. Bhowmik, Omar Noori, Si L. Chen, Haesook Han, Michael R. Fisch, Christina M. Robb, Aaron Variyam, Alfonso Martinez-Felipe

PII: S0167-7322(21)00096-9

DOI: https://doi.org/10.1016/j.molliq.2021.115370

Reference: MOLLIQ 115370

To appear in: *Journal of Molecular Liquids*

Received date: 23 November 2020

Revised date: 6 January 2021

Accepted date: 9 January 2021

Please cite this article as: P.K. Bhowmik, O. Noori, S.L. Chen, et al., Ionic liquid crystals: Synthesis and characterization via NMR, DSC, POM, X-ray diffraction and ionic conductivity of asymmetric viologen bistriflimide salts, *Journal of Molecular Liquids* (2021), https://doi.org/10.1016/j.molliq.2021.115370

# Ionic liquid crystals: synthesis and characterization via NMR, DSC, POM, X-ray diffraction and ionic conductivity of asymmetric viologen bistriflimide salts

Pradip K. Bhowmik,[a] Omar Noori,[a] Si L. Chen,[a] Haesook Han[a]

[a]*Department of Chemistry and Biochemistry, University of Nevada Las Vegas, 4505 S. Maryland Parkway, Box 454003, Las Vegas, NV 89154, USA*. Phone: (702) 895-0885; Fax: (702) 895-4072; Email: pradip.bhowmik@unlv.edu

Michael R. Fisch,[b] Christina M. Robb[c]

[b]*College of Aeronautics and Engineering, Kent State University, Kent, OH 44242, USA.*

[c]*Department of Chemistry, Kent State University, Kent, OH 44242, USA.*

Aaron Variyam[d], and Alfonso Martinez-Felipe[d]

[d]*Chemical and Materials Engineering Group, School of Engineering, University of Aberdeen, King's College, Old Aberdeen, AB24 3UE, UK.*

ABSTRACT

A series of asymmetric viologen bistriflimide salts of both short and long alkyl chains were synthesized by the metathesis reaction of lithium triflimide salt with the respective asymmetric viologen dibromide salts in methanol. Their thermotropic liquid crystalline were determined by differential scanning calorimetry, polarizing optical microscopy and variable temperature X-ray diffraction techniques. These salts melt into highly-ordered smectic T phases that is, crystal-to SmT transitions ($T_m$s) at relatively low temperatures (lowest $T_m$ at -12 ℃) and maintain liquid crystallinity in a wide range of temperatures (8-132 ℃), with excellent thermal stabilities up to 320 ℃ as determined by thermogravimetric analysis. These results differ with respect to the symmetric viologen bistriflimide salts. Ionic conductivity of these salts was also

measured by dielectric impedance spectroscopy and found to be in the $10^{-2.43}$ S $cm^{-1}$ range, highlighting their potential as electrolytes at room temperature.

*Keywords:* ionic liquid crystals; differential scanning calorimetry; polarizing optical microscopy; variable temperature X-ray diffraction; smectic T phase; ionic conductivity

## 1. Introduction

The 1,1′-dialkyl-4,4′-bipyridinium salts are commonly known as viologens. They are an important class of dicationic salts and are considered as advanced functional materials, due to their unique properties including, redox performance, ionic conductivity, thermochromism, photochromism, electrochromism and piezochromism [1]. Among others, viologens can be applied as electrochromic devices, molecular machines, organic batteries, and carbohydrate oxidation catalysts in alkaline fuel cells [2-4]. Viologens have contributed to populate an emerging variety of ionic liquids by introducing chemical modifications of cations and anions [5-13], and are excellent candidates to prepare new ionic liquid crystals (ILCs), due to their rod-like core and flexible terminations [8, 14-25]. Recently, we reported the LC properties of a series of symmetric viologens with triflimide as a counterion, which were highly dependent on the alkyl chain length ($n$= 1-20) [18-20]. More specifically, compounds with $n$ = 6, 7 and 8 showed SmA phases, whilst those with higher alkyl chain lengths ($n$ = 14, 16, 18 and 20) formed SmC and SmA phases, and an unidentified (SmX) phase. The rest of compounds behaved as salts melting into ionic liquids at high temperatures. In contrast, Causin and Saielli [8] reported that slightly asymmetric viologen bistriflimide salts exhibit a smectic phase with a wide range of stability that range varying from 0℃ to 146 ℃, whilst LC behavior is inhibited in strongly asymmetric viologen salts, which have rather low melting transitions just below 40 ℃. For example, an asymmetric viologen salt (7BP11) shows a crystal-to-LC transition ($T_m$) at 0℃ and LC-to-

isotropic transition ($T_i$) at 136℃ thus resulting in the LC phase region of 136 ℃. Similarly, another salt of this type (8BP10) shows a $T_m$ at 4 ℃ and $T_i$ at 146 ℃ thus resulting in the LC phase region of 142 ℃. The majority of the asymmetric viologen salts reported in that study contained heptyl terminal groups (7BP*n*, with *n* = 8, 9, 10 and 11), and octyl terminal groups (8BP*n*, with *n* = 5, 6, 8, 9, 10 and 11), and only two slightly asymmetric compounds having hexyl group (6BP*n*, with *n* = 8 and 9) were included.

To explore how to stabilize the mesomorphism in asymmetric ILCs, herein, we describe the properties of an extended series of asymmetric bistriflimide viologen salts with hexyl terminal groups and different alkyl chain lengths (6BP*n*, with *n* = 5, 7, 10, 11, 12, 14, 16, 18 and 20). We have assessed their chemical structures by $^{1}H$ and $^{13}C$ NMR spectroscopy and elemental analysis, and have determined their thermal stabilities by thermogravimetric analysis (TGA). We have then characterized their liquid crystalline phase behaviour and structures by a combination of differential scanning calorimetry (DSC), polarizing optical microscopy (POM) and variable temperature X-ray diffraction (VT-XRD) studies. The general structures and designations for these newly synthesized asymmetric viologen bistriflimide salts, and their synthetic routes, are shown in Scheme 1. We have analysed structure-property relationship on our ILCs, by considering two main groups: those containing short (*n* = 5, 7, 10 and 11) and long (*n* = 12, 14, 16, 18 and 20) alkyl chain lengths. Additionally, we have also correlated the composition of our ILCs with their dielectric and ionic conductivity response, using electrochemical impedance spectroscopy, in a broad range of frequencies and temperatures. During the last few decades, it has been shown that liquid crystallinity can enhance ionic conductivity, by a combination of long-range order and short-order mobility, and their self-healing properties and flexibility make them attractive electrolytes in batteries, solar cells, and

fuel cells [26-40]. Here, we investigate whether similar mechanisms can take place through our ILCs. Furthermore, they exhibit LC phases even below room temperature (ca. -10 ℃) to as high as ca. 150 ℃ thus enabling the very broad range of LC phases, they could be potentially suitable as ordered reaction media for carrying out in many organic reactions with high yields and selectivity including Diels-Alder reactions and intramolecular Diels-Alder reactions [41-44].

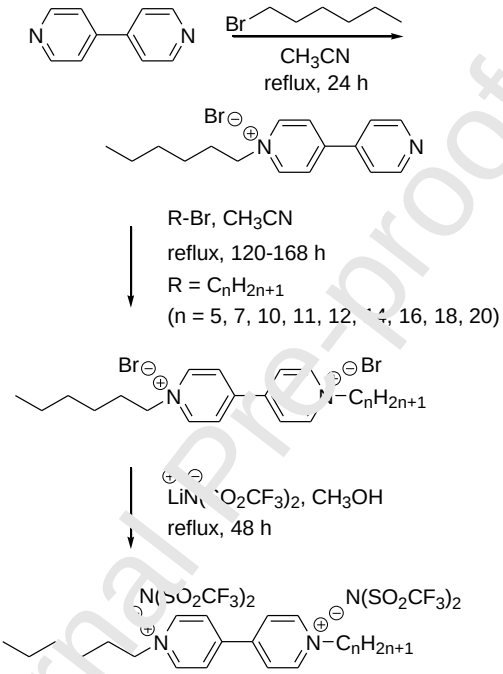


**(6BP5, 6BP7, 6BP10, 6BP11, 6BP12, 6BP14, 6BP16, 6BP18, 6BP20)**

**Scheme 1.** Synthetic routes for the asymmetric viologen bistriflimide salts of a 4,4′-bipyridinium core (BP) alkylated with hexyl group with *n* = 5, 7, 10, 11, 12, 14, 16, 18 and 20.

## 2. Materials and methods

### *2.1 General Information*

All chemicals and solvents were reagent grade, were obtained from Alfa Aesar, Sigma Aldrich or Acros Chemical Co., and were used received. The $^{1}H$ and $^{13}C$ nuclear magnetic resonance (NMR) spectra of all the symmetric viologen salts in $CD_3OD$ were recorded by using VNMR 400 spectrometer operating at 400 and 100 MHz at room temperature. Elemental

analysis was performed by Atlanta Microlab Inc., Norcross, GA. Differential scanning calorimetry (DSC) measurements of all the compounds were conducted on TA module DSC Q200 series in nitrogen at heating and cooling rates of 10 $^{o}$C/min. The temperature axis of the DSC thermograms was calibrated before use with reference standards of high purity indium and tin. Their thermogravimetric analyses (TGA) were performed using a TGA Q50 instrument at a heating rate of 10 ºC/min in nitrogen. Optical studies were performed on these asymmetric viologen salts sandwiched between a standard microscope glass slide and coverslip. The samples were heated and cooled on a Mettler hot stage (FP82HT) and (FP90) controller and observations of the phases made between crossed polarizers of an Olympus BX51 microscope. In short, salts were heated above their clearing transitions and cooled at 5 °C/min to room temperature, with brief pauses to collect images and observe specific transitions.

X-ray diffraction studies of salts contained in flame sealed 1 mm quartz capillaries were performed using a Rigaku Screen Machine. The salt under study was placed inside the Linkam HFS350X-Cap capillary hot stage 72 mm away from the 2D detector, with temperature controlled to the accuracy of ± 0.1°C. A magnetic field of ~2.5kG was applied to the samples using a pair of samarium cobalt permanent magnets (with B nearly parallel to the beamstop visible as a vertical line in diffraction images). Scattering patterns were collected using a Mercury 3 CCD detector with resolution 1024×1024 pixels (size: 73.2 μm×73.2 μm) and copper $K_\alpha$ radiation generated by a microfocus sealed X-ray tube with copper anode ($\lambda$ = 1.542 Å). The data were analyzed using publicly available Fit-2D software to correct for background scattering and generate intensity vs scattering vector, I-q curves. The intensity spectra exhibit several peaks. These peaks were fit to a Lorentzian form (or a sum of Lorentzians) as appropriate using a least squares fitting routine written in Mathematica. The outputs of the program include the

location of the peak, $q_0$ and the half width at half maximum, $\Delta q$. The characteristics distances were found from $q_0$ as $r = \frac{2\pi}{q_0}$.

The conductivity of the C6BPCn(s) was studied by complex impedance spectroscopy. Indium Tin Oxide cells, ITO (SG100A080uG180, Instec), were filled by capillary with the samples in the melt state, to yield anti-parallel alignments with 1° to 3° pre-tilted angles, as confirmed by POM. Cells had $A = 100\ mm^2$ active areas, with 100 Ω resistance and $v = 8\ \mu m$ thickness, and their capacitance, $C_O$, was then calculated as,

$$C_O = \varepsilon_O \frac{A}{v} = 1.10675 * 10^{-9} F$$

where $\varepsilon_O = 8.854 \cdot 10^{-12}\ F \cdot m^{-1}$, is the dielectric permittivity of vacuum.

A PARSTAT MC multichannel potentiostat (Ametek) was connected to the cells, which were then placed on a Linkham TMS 91 hot stage for temperature control, with ±0.1 $^{o}$C accuracy. The dielectric response was measured in isothermal frequency sweeps between $10^6$ Hz and 0.1 Hz, applying $V_{rms}$= 1000 mV amplitude alternating electric fields in the absence of bias electric fields ($V_{bias}$ = 0 V).

The results have been analyzed in terms of the complex permittivity, $\varepsilon^*(\omega) = \varepsilon' - j\varepsilon''$, and conductivity, $\sigma^*(\omega) = \sigma' + j\sigma''$, measured as a function of the frequency, w (rad·s$^{-1}$), and the temperature, *T*, with $j$ is the imaginary unit, $\sqrt{-1}$. More specifically, the complex permittivity, was calculated from the complex impedance $Z^* = Z' + jZ''$, according to,

$$\varepsilon^* = \frac{1}{j\omega C_O Z^*} \qquad \text{Eq. 1}$$

and the elastic permittivity, $\varepsilon' = \frac{Z''}{\omega C_O |Z|}$, and dielectric loss factor, $\varepsilon'' = \frac{Z'}{\omega C_O |Z|}$, were obtained.

The complex conductivity of the samples was then calculated as [45],

$$\sigma^* = \varepsilon^* \varepsilon_0 \omega \qquad \text{Eq. 2}$$

with $\sigma' = \omega\epsilon_0\varepsilon''$ and $\sigma'' = \omega\epsilon_0\varepsilon'$ .

The complex electric modulus, $M^*(\omega) = M' + jM''$, was also studied, to discriminate polarization and conductive effects [46],

$$M^* = \frac{1}{\varepsilon^*} = \frac{1}{\varepsilon' - \varepsilon''} = \frac{\varepsilon'}{\varepsilon'^2 + \varepsilon''^2} + j\frac{\varepsilon''}{\varepsilon'^2 + \varepsilon''^2} \qquad \text{Eq. 3}$$

with $M' = \frac{\varepsilon'}{\varepsilon'^2 + \varepsilon''^2}$ and $M'' = \frac{\varepsilon''}{\varepsilon'^2 + \varepsilon''^2}$.

Unless stated otherwise, the results will be displayed as a function of the frequency in Hertz, with $f = \omega / 2\pi$.

*2.2 Synthesis*

2.2.1. *Preparation of 1-hexyl-4,4′-bipyridinium bromide (6BP6Br)*

The 4, 4′-bipyridine (0.821g, 1.69 mmol) was dissolved in 25 mL of acetonitrile (ACN); 1-bromohexane, (0.335 g, 2.03 mmol) were added dropwise slowly to the reaction flask and the solution was heated in an oil bath at 81 °C for 24 h . Reaction was monitored using an alumina TLC plate and an eluant of a mixture of acetone and methanol (4/1, v/v). Once the reaction was complete, the reaction was turned off and reaction content was air-filtered to remove yellow dialkylated product. Acetonitrile was removed from the filtrate using a rotary evaporator to yield the crude product which was then washed with toluene. Finally, it was purified by using an alumina column chromatography and an eluent of a mixture acetone and methanol (4/1 v/v) giving a pure light gray/white compound (0.346 g, 1.10 mmol, yield 64%). $\delta_H$ ($CD_3OD$, 400 MHz, ppm): 9.14-9.16 (2H, d, *J* = 6.8 Hz), 8.83-8.85 (2H, dd, *J* = 1.7 Hz, *J* = 4.7 Hz), 8.53-8.55 (2H, d, J = 6.8 Hz), 8.00-8.02 (2H, dd, J = 1.7 Hz, J = 4.7 Hz), 4.69-4.72 (2H, t, *J* = 7.2 Hz), 2.05-2.12 (2H, m), 1.36-1.48 (6H, m) 0.92-0.96 (3H, m).

*2.2.2. Preparation of 1-hexyl-1′-pentyl-4,4′-bipyridinium dibromide (6BP5Br$_2$)*

An amount of **6BPBr** (0.500 g, 1.56 mmol) and excess of 1-bromopentane (0.571 g, 3.42 mmol) were added to 5 mL of ACN and heated to reflux for 120 h. The completion of the reaction was monitored by using an alumina gel thin layer chromatography and an eluent of a mixture of acetone and methanol (4/1 v/v). The reaction mixture was then cooled to room temperature (rt) and the crude product was collected by filtration. It was purified by simply washing with ACN and hexane, respectively, giving the pure product (0.656 g, 1.39 mmol, yield = 89%). $\delta_H$ ($CD_3OD$, 400 MHz, ppm): 9.29-9.31 (4H, d, *J* = 6.8 Hz), 8.70-8.71 (4H, d, *J* = 6.4 Hz), 4.75-4.79 (4H, t, *J* = 7.6 Hz), 2.09-2.13 (4H, m), 1.39-1.47 (10H, m) 0.92-0.99 (6H, m).

*2.2.3. Preparation of 1-hexyl-1-pentyl-4,4′-bipyridinium dibis(trifluoromethanesulfonyl)imide] (6BP5)*

The metathesis reaction was performed according to the known procedures [18-20]. The typical procedure was described as follows. An amount of **$6BP5Br_2$** (0.500 g, 1.06 mmol) was dissolved in 15 mL of methanol on heating. 5 mL of a methanol solution of $LiNTf_2$ (0.699 g, 2.33 mmol) was then added slowly dropwise over a period of two min. The reaction flask was then heated to reflux for 48 h. At the end of the reaction period, methanol was removed using a rotary evaporator. 30 mL of water was added and heated to boiling resulting in liquid product, which was then decanted to get the crude product. It was then washed repeatedly with water and dried in vacuum oven at 80 °C giving the desired product (0.774 g, 0.89 mmol, yield = 84%). For the solid product, it was precipitated out, filtered, washed with water and dried in vacuum at 80 °C giving the desired product. The typical yields of asymmetric viologen triflimides of the metathesis reaction were in the range of 77-96%.

Typical data for **6BP5:** $\delta_H$ ($CD_3OD$, 400 MHz, ppm): 9.23-9.24 (4H, d, *J* = 6.8 Hz), 8.62-8.63 (4H, d, *J* = 6.4 Hz), 4.71-4.74 (4H, t, *J* = 7.6 Hz), 2.07-2.10 (4H, m), 1.38-1.45 (10H, m), 0.91-0.98 (6H, m). $\delta_C$ ($CD_3OD$, 400 MHz, ppm): 151.47, 147.08, 128.35, 125.98, 122.80, 119.61,

116.42, 63.40, 32.56, 32.32, 32.29, 29.31, 26.92, 23.48, 23.20, 14.28, 14.13. Anal. calcd for $C_{25}H_{32}N_4O_8F_{12}S_4$ (872.78): C, 34.40; H, 3.70; N, 6.42; S, 14.70%. Found C, 34.49; H, 3.71; N, 6.28; S, 14.42%.

Data for **6BP7:** Yield 94%. $\delta_H$ ($CD_3OD$, 400 MHz, ppm): 9.22-9.24 (4H, d, *J* = 6.8 Hz), 8.61-8.63 (4H, d, *J* = 6.4 Hz), 4.71-4.74 (4H, t, *J* = 7.6 Hz), 2.05-2.11 (4H, m), 1.33-1.43 (14H, m), 0.89-0.94 (6H, m). $\delta_C$ ($CD_3OD$, 400 MHz, ppm): 151.47, 147.06, 128.35, 125.98, 122.79, 119.60, 116.41, 63.41, 32.72, 32.59, 32.55, 32.32, 29.83, 27.20, 26.91, 23.61, 23.48, 14.37, 14.28. Anal. calcd for $C_{27}H_{36}N_4O_8F_{12}S_4$ (900.84): C, 36.00; H, 4.03; N, 6.22; S, 14.24%. Found C, 36.12; H, 3.93; N, 6.23; S, 13.98%.

Data for **6BP10:** Yield 94%. $\delta_H$ ($CD_3OD$, 400 MHz, ppm): 9.22-9.24 (4H, d, *J* = 6.8 Hz), 8.61-8.63 (4H, d, *J* = 6.4 Hz), 4.71-4.74 (4H, t, *J* = 7.6 Hz), 2.05-2.12 (4H, m), 1.29-1.43 (20H, m), 0.88-0.94 (6H, m). $\delta_C$ ($CD_3OD$, 400 MHz, ppm): 151.47, 147.13, 128.35, 125.98, 122.78, 119.60, 116.41, 63.42, 33.06, 32.60, 32.55, 32.32, 30.62, 30.51, 30.42, 30.16, 27.24, 26.91, 23.75, 23.48, 14.45, 14.28. Anal. calcd for $C_{30}H_{42}N_4O_8F_{12}S_4$ (942.92): C, 38.21; H, 4.49; N, 5.94; S, 13.60%. Found C, 38.16; H, 4.38; N, 5.93; S, 13.39%.

Data for **6BP11:** Yield 95%. $\delta_H$ ($CD_3OD$, 400 MHz, ppm): 9.21-9.23 (4H, d, *J* = 6.4 Hz), 8.60-8.62 (4H, d, *J* = 6.8 Hz), 4.70-4.74 (4H, t, *J* = 7.6 Hz), 2.05-2.12 (4H, m), 1.29-1.43 (22H, m), 0.88-0.94 (6H, m). $\delta_C$ ($CD_3OD$, 400 MHz, ppm): 151.46, 147.10, 128.36, 125.96, 122.78, 119.59, 116.40, 63.41, 33.08, 32.58, 32.53, 32.30, 30.70, 30.66, 30.49, 30.46, 30.15, 27.23, 26.89, 23.75, 23.46, 14.46, 14.28. Anal. calcd for $C_{31}H_{44}N_4O_8F_{12}S_4$ (956.94): C, 38.91; H, 4.63; N, 5.85; S, 13.40%. Found C, 38.67; H, 4.62; N, 5.84; S, 13.43%.

Data for **6BP12:** Yield 79%. $\delta_H$ ($CD_3OD$, 400 MHz, ppm): 9.23-9.22 (4H, d, *J* = 6.4 Hz), 8.61-8.62 (4H, d, *J* = 6.4 Hz), 4.70-4.74 (4H, t, *J* = 7.6 Hz), 2.05-2.12 (4H, m), 1.29-1.43 (24H, m),

0.88-0.91 (6H, m). $\delta_C$ ($CD_3OD$, 400 MHz, ppm): 149.97, 145.56, 126.87, 124.48, 121.29, 118.10, 114.92, 61.93, 31.61, 31.10, 31.05, 30.82, 29.62, 29.17, 29.01, 28.67, 25.75, 25.41, 22.27, 21.98, 12.98, 12.80. Anal. calcd for $C_{32}H_{46}N_4O_8F_{12}S_4$ (970.97): C, 39.58; H, 4.78; N, 5.77; S, 13.21%. Found C, 39.55; H, 4.59; N, 5.85; S, 12.93%.

Data for **6BP14:** Yield 77%. $\delta_H$ ($CD_3OD$, 400 MHz, ppm): 9.22-9.24 (4H, d, *J* = 6.8 Hz), 8.61-8.63 (4H, d, *J* = 6.4 Hz), 4.70-4.74 (4H, t, *J* = 7.6 Hz), 2.04-2.12 (4H, m), 1.28-1.42 (28H, m), 0.88-0.94 (6H, m). $\delta_C$ ($CD_3OD$, 400 MHz, ppm): 151.46, 147.03, 128.35, 125.98, 122.79, 119.60, 116.41, 63.41, 33.11, 32.60, 32.54, 32.32, 30.82, 30.78, 30.75, 30.67, 30.50, 30.17, 27.25, 26.91, 23.77, 23.48, 14.47, 14.28. Anal. calcd for $C_{34}H_{50}N_4O_8F_{12}S_4$ (999.02): C, 40.88; H, 5.04; N, 5.61; S, 12.84%. Found C, 40.83; H, 4.92; N, 5.61, S, 12.99%.

Data for **6BP16:** Yield 78%. $\delta_H$ ($CD_3OD$, 400 MHz, ppm): 9.25-9.23 (4H, d, *J* = 6.8 Hz), 8.62-8.64 (4H, d, *J* = 6.4 Hz), 4.71-4.74 (4H, t, *J* = 7.6 Hz), 2.05-2.12 (4H, m), 1.28-1.43 (32H, m), 0.88-0.94 (6H, m). $\delta_C$ ($CD_3OD$, 400 MHz, ppm): 151.46, 147.04, 128.35, 125.97, 122.78, 119.59, 116.41, 63.41, 33.10, 32.59, 32.54, 32.31, 30.83, 30.82, 30.79, 30.67, 30.50, 30.17, 27.25, 26.90, 23.77, 23.47, 14.47, 14.28. Anal. calcd for $C_{36}H_{54}N_4O_8F_{12}S_4$ (1027.08): C, 42.10; H, 5.30; N, 5.45; S, 12.49%. Found C, 42.36; H, 5.45; N, 5.54; S, 12.51%.

Data for **6BP18:** Yield 90%. $\delta_H$ ($CD_3OD$, 400 MHz, ppm): 9.13-9.12 (4H, d, *J* = 6.0 Hz), 8.51-8.53 (4H, d, *J* = 6.8 Hz), 4.61-4.64 (4H, t, *J* = 7.6 Hz), 1.95-2.02 (4H, m), 1.26-1.33 (36H, m), 0.78-0.85 (6H, m). $\delta_C$ ($CD_3OD$, 400 MHz, ppm): 149.99, 145.58, 126.88, 124.50, 121.31, 118.12, 114.94, 61.95, 31.64, 31.13, 31.07, 30.84, 29.35, 29.32, 29.29, 29.21, 29.04, 28.70, 25.78, 25.43, 22.30, 22.00, 13.01, 12.82. Anal. calcd for $C_{38}H_{58}N_4O_8F_{12}S_4$ (1055.13): C, 43.26; H, 5.54; N, 5.31; S, 12.16%. Found C, 43.23; H, 5.57; N, 5.25; S, 12.23%.

Data for **6BP20:** Yield 87%. $\delta_H$ ($CD_3OD$, 400 MHz, ppm): 9.21-9.23 (4H, d, *J* = 6.4 Hz), 8.61-8.62 (4H, d, *J* = 6.8 Hz), 4.70-4.74 (4H, t, *J* = 7.6 Hz), 2.04-2.10 (4H, m), 1.28-1.42 (40H, m), 0.88-0.94 (6H, m). $\delta_C$ ($CD_3OD$, 400 MHz, ppm): 149.99, 145.58, 126.88, 124.50, 121.32, 118.13, 114.94, 61.95, 31.64, 31.13, 31.07, 30.84, 29.35, 29.33, 29.30, 29.21, 29.04, 28.70, 25.78, 25.43, 22.31, 22.00, 13.01, 12.82. Anal. calcd for $C_{40}H_{62}N_4O_8F_{12}S_4$ (1083.18): C, 44.35; H, 5.77; N, 5.17; S, 11.84%. Found C, 44.53; H, 5.95; N, 5.24; S, 11.75%.

## 3. Results and discussion

### *3.1 Synthesis of asymmetric viologen bistriflimide salts (6BP5-20)*

In short, the synthesis of these salts involved essentially three steps. Firstly, preparation of 1-hexyl-4,4′-bipyridinium bromide (BP6Br), which was prepared by reacting 4,4′-bipyridine with 1-hexyl bromide on heating to reflux for 24 h in acetonitrile. A second step consisted on the reaction of BP6Br with the respective 1-alkyl bromides, under reflux for 120-168 h, again in acetonitrile, to produce the asymmetric dibromide compound. The third and last step was the exchange of the respective dibromides with the lithium bistriflimide salt, under reflux for 48 h in methanol (Scheme 1), according previously reported procedures [18-20]. The typical procedure corresponding to the preparation of 6BP5 bistriflimide is described with detail in the Experimental section. Other salts were prepared following analogous procedures [18-20]. The composition and purity of the intermediates and products were determined from the $^1H$ and $^{13}C$ NMR spectra (Fig. S1-Fig. S9) and elemental analysis, and representative data are also included in the Experimental section.

### *3.2 Thermotropic LC properties of 6BPn by DSC, POM and VT-XRD*

The thermotropic LC properties of 6BPn were examined by experimental techniques including DSC, POM and VT-XRD [47-51]. Fig. 1 shows the DSC thermograms of 6BP12

obtained at heating and cooling rates of 10 ℃·min$^{-1}$, as a representative example of the asymmetric viologen salts with short alkyl chains, see Fig. S10-Fig. S13. The thermal parameters obtained from the DSC results for all the samples are summarized in Table 1, and are in excellent agreement with our POM observations. Two endotherms are visible in all heating and cooling cycles of these samples, corresponding to first-order phase transitions. The two transitions have similar enthalpy changes, and correspond to crystal-to-LC ($T_m$) and LC-to-isotropic ($T_i$) transitions (clearing), in increasing temperature order. 6BP12 exhibits the lowest melting point of this series, with $T_m$ = -12 ℃, and has the largest LC phase range of the series, $\Delta T_{LC}$ = 132 ℃. Generally, enthalpy values calculated for melting transitions were higher than for clearing transitions ($\Delta H_m > \Delta H_i$). Viologens with longer terminal chains, 6BP14, 6BP18 and 6BP20, on the other hand, display an additional endotherm below the $T_m$ transition, which can be associated with a crystal-to-crystal transition (Fig. S14-Fig. S17) [52-56]. The existence of crystal polymorphism was verified on observation of highly birefringent textures, including defects and absence of homogeneity.

Both $T_m$ and $\Delta H_m$ decreased at longer alkyl terminations lengths up to 6BP12, being in excellent agreement with those of other asymmetric viologen salts [8]. After reaching a minimum for n=12 (6BP12), $T_m$ and $\Delta H_m$ subsequently increase with *n*, for these homologues with longer chains (6BP14-6BP20). We note that it is possible to yield asymmetric viologen salts exhibited $T_m$ not only at room temperature but also at well below rt. Keeping one alkyl chain length n = 6 constant, the $T_m$ gradually decreased with the increase with the increase in carbon atoms of the alkyl chain up to n =12 and then increased gradually with the further increase in carbon atoms of the alkyl chain (n =14, 16,18, 20). These results are in excellent agreement with those of other ILCs reported in the literature [26,32,57,58]. The $T_i$ tends to increase with longer

alkyl chains, following an odd-even effect, visible in the lower end of *n* values (Fig. 2). These results also reflect a better packing efficiency of *trans*-configurations in odd membered viologens, which can accommodate molecular arrangements more compatible with liquid crystalline phases than the even-membered analogous. Whilst the enthalpy change for this transition did not follow any regular trend with *n*, falling in the range of 0.5-9.7 $kJ \cdot mol^{-1}$, it is worth mentioning that $\Delta H_i$ was the lowest for 6BP5, and the highest for 6BP16. Interestingly, the LC phase range ($\Delta T_{LC} = T_i - T_m$) varied remarkably with composition (Fig. 3), from $\Delta T_{LC} = 8$ (for 6BP5), to $\Delta T_{LC} =$ 132 °C (for 6BP12).

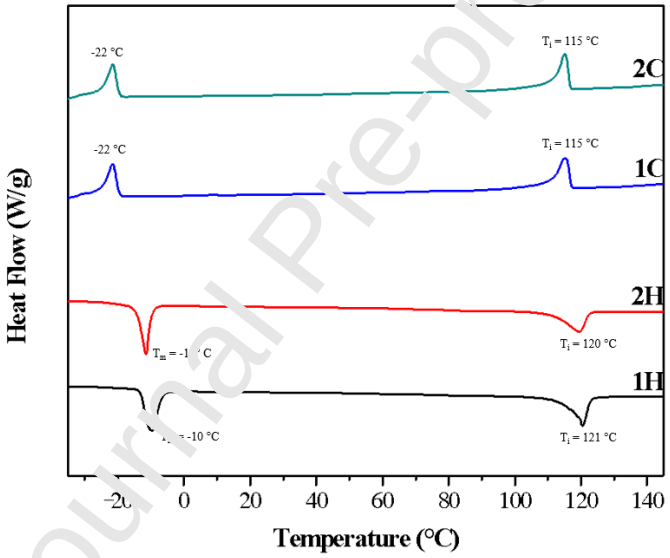


**Fig. 1** DSC thermograms of **C6BPC12** obtained at heating and cooling rates of 10 °C/min in nitrogen.

Fig. 4 shows representative textures observed under the polarizing optical microscope, POM, on cooling these salts from their isotropic melts, including the presence of homeotropic regions typical of ILCs. Unfortunately, these textures were not useful to unambiguously identify the mesophases formed, and phase identification was not possible from visual observation. We can, however, rule out the presence of smectic phases of low order, such as, SmA and SmC, due

to the absence of Schlieren, focal conic, oily-streaks, or broken focal textures. Hence, VT-XRD studies of these salts were performed to determine the nature of these ordered LC phases, and Fig. 5 shows an example of the results obtained for 6BP16.

**Table 1.** Thermodynamic properties of phase transition temperatures of asymmetric viologen bistriflimide salts (6BPn) obtained from DSC measurements and decomposition temperatures obtained from TGA measurements

| Sample | $T_m$ [a] °C ($\Delta H_m$ /kJ·mol$^{-1}$) | $T_i$ [b] °C ($\Delta H_i$ /kJ·mol$^{-1}$) | $\Delta T$ [c] °C | $T_d$ [d] °C |
|---|---|---|---|---|
| 6BP5 | 28 (13.6) | 36 (0.5) | 8 | 337 |
| 6BP6[e] | 58 | 78 | 20 | 362 |
| 6BP7 | 30 (14.1) | 88 (5.6) | 58 | 334 |
| 6BP8[f] | 24 (12.1) | 103.8 (8.1) | 80 | n/a |
| 6BP9[f] | 8.2 (14.0) | 106.2 (9.1) | 98 | n/a |
| 6BP10 | 0 (12.3) | 114 (9.1) | 114 | 337 |
| 6BP11 | -11 (7.1) | 98 (8.6) | 109 | 333 |
| 6BP12 | -12 (6.9) | 120 (6.6) | 132 | 331 |
| 6BP14 | 27 (23.4) | 132 (9.1) | 105 | 329 |
| 6BP16 | 42 (46.7) | 144 (9.7) | 102 | 335 |
| 6BP18 | 45[g] (26.6), 54 (20.5) | 145 (5.3) | 91 | 335 |
| 6BP20 | 45[g] (24.0), 67 (27.6) | 151 (4.8) | 84 | 332 |

[a] $T_m$ = Crystal-to-LC phase transition. Datum was taken from the second heating cycle of the DSC thermogram at a heating rate of 10 °C/min. The value in the parentheses was the enthalpy in kJ/mol for this transition.

[b] $T_i$ = LC-to Isotropic transition. Datum was taken from the second heating cycle of the DSC thermogram at a heating rate of 10 °C/min.

[c] $\Delta T = (T_i - T_m)$, that is, the LC phase range.

[d] $T_d$ = The temperature at which a 5% weight loss of the salt occurred at a heating rate of 10 °C/min in nitrogen.

[e] From Reference [19].

[f] From Reference [8].

[g] Crystal-to-crystal transition. Datum was taken from the second heating cycle of the DSC thermogram at a heating rate of 10 °C/min.

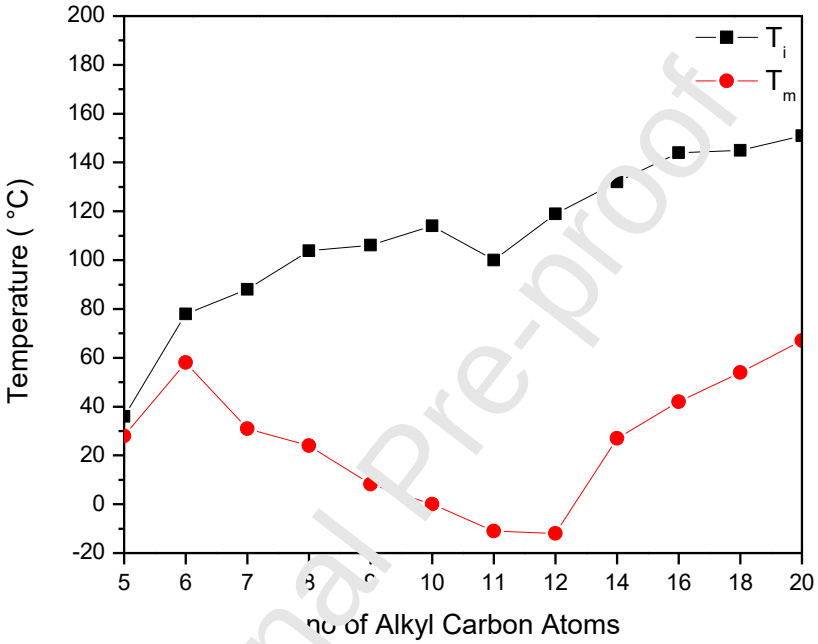


**Fig. 2** $T_m$ and $T_i$ dependences of 5BPn as a function of alkyl carbon chain length (n).

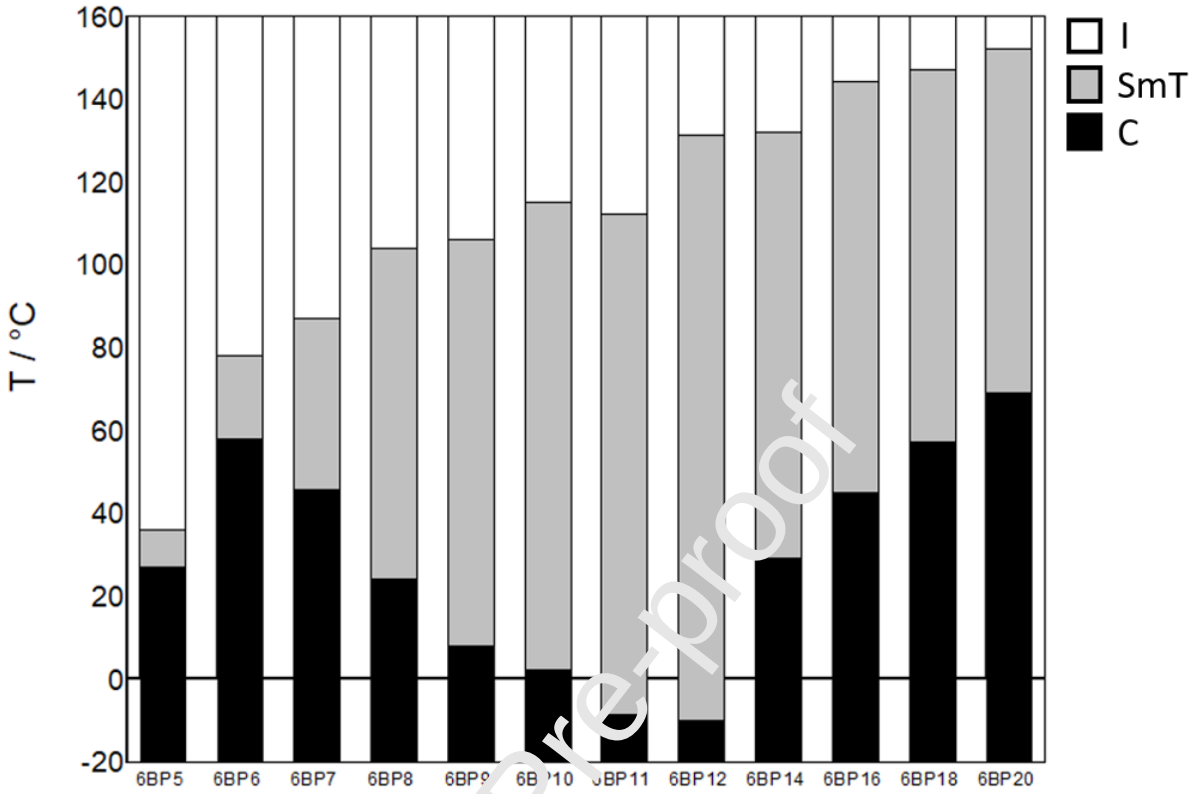


**Fig. 3** Range of LC phases of various asymmetric viologen bistriflimide studied in this work, of 6BP8 and 6BP9 [8] and of symmetric 6BP6 [19]. I = isotropic liquid (light gray); SmT = smectic phase T (gray); and C = crystal (black).

(a)

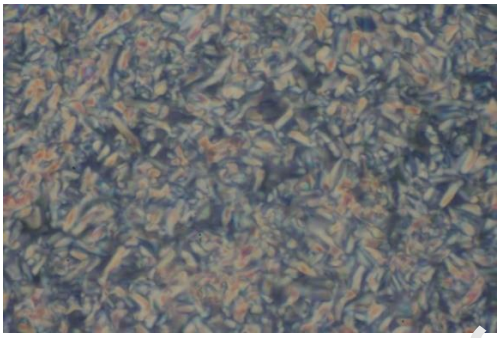

(b)

(c)

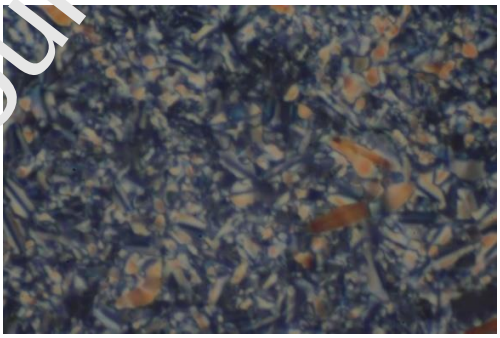



**Fig. 4** Typical textures taken by POM studies revealing unidentifiable textures of (a) 6BP12 at 110 °C (b) 6BP14 at 120 °C and (c) 6BP16 130 °C on cooling their respective isotropic phases

suggestive of their smectic T phases (magnification 400 ×) as determined by VT-XRD (*vide infra*).

Fig. 5 shows sharp peaks in the LC range of 6BP16. The peaks have been indexed on the graph and the lowest temperature scan. The long axis of the molecule is parallel to the third index and the first two are within the plane perpendicular to the axis. In the wide-angle region, there are two very clear peaks. They are labelled 110 and 200. The 100 peak is visible on some scans, but very weak. The 110 peak shows two peaks as indicated in the graph and the pictures of scans. These two peaks are at $\boldsymbol{d_{110} \approx 5.2}$ Å $\boldsymbol{and\ d_{200} \approx 7.3}$ Å. The size and sharpness indicate that the chains have crystallized, and their ratio, $\mathrm{d}/\boldsymbol{d} = \sqrt{2}$, the existence of a square lattice. In practice the ratio was very close to 1.41. A tetrahedral lattice has lattice spacings in the plane given by $\frac{\mathbf{1}}{\boldsymbol{d_{hk0}^2}} = \frac{\boldsymbol{h^2+k^2}}{\boldsymbol{a^2}}$ where *d* is the spacing, *h* and *k* are integers and *a* the in-plane lattice spacing. Similar tetragonal structures were discovered by Arkas and coworkers [59] in dihydroxy ethyl derivatives of quaternary alkylammonium bromide salts and Ohta and coworkers [60] in 1,4-dialkyl-1,4-diazoniabibyclo[2.2.2]octane dibromides, and were identified as smectic T phases (SmT). The small angle peaks corresponding to longer distances are also consistent with this phase assignation and the presence of well-defined layers. In the LC phase, there are two sharp signals at $\boldsymbol{d \approx 24}$ Å and $\mathrm{d} \approx \mathbf{12}$ Å that are harmonically related. In the crystal phase, additional bands appear at $\boldsymbol{d \approx 48}$ Å, $\mathrm{d} \approx \mathbf{16}$ Å and $\boldsymbol{d \approx 9.8}$ Å. Corresponding to harmonics that evidence very strong layer ordering. Similarly, the characteristic d-spacings and *I* versus *q* scattering plots of 6BP7, 6BP10, 6BP11, 6BP12, 6BP14, 6BP18 and 6BP20 are given in Fig. S18- Fig. S25, and all

are consistent with the formation of SmT phases. These results are consistent with non-symmetric pyrrolidinium-based ILCs containing bromide, tetrafluoroborate and

hexafluorophosphate [61] as well as laterally substituted quaternary ammonium bromide ILC [62]. Additionally, Yang and coworkers [63] reported that diimadazolium-based ILCs containing tetrafluoroborate, hexafluorophosphate, perchlorate and bis(triflimide), show SmT phases. Do and Schmitzer [42]

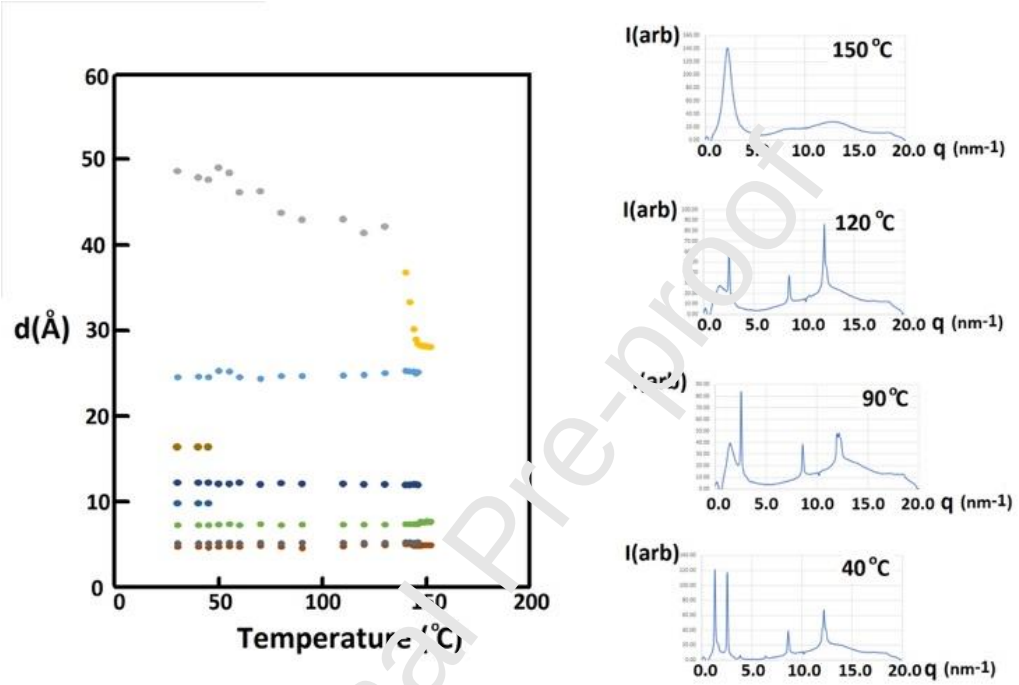


**Fig. 5** Characteristic d-spacings and representative *I* versus *q* scattering plots of 6BP16 at different temperatures. The different coloured symbols indicate a line that started or ended at a specific temperature.

also found that this phase is also present in dialkyl(1,5-naphthalene)diimidazolium bis(triflimide) salts (n = 12, 16). We note here that the symmetric viologen bistriflimide salts studied in the previous reports display a more complex phase behaviour respect to the alkyl chain length, including SmA phases (n= 6, 7, 8), no mesomorphism (n = 9, 10, 11, 12) and (unidentified) SmX, SmC and SmA phases (n =14, 16, 18, 20) [18-20].

Most of the ILCs reported in the literature show SmA phases and some show both SmC and SmA phases of low order, due to nano-segregation of the polar ionic groups and nonpolar hydrophobic alkyl groups, and giving rise to layer structures in which hydrophobic layers alternate with ionic layers [26,32,57,58,64,65]. In rare instances, ILCs can also show SmB [8], SmT [42,59-63] and SmH [66] phases of higher order. It is not uncommon for LC homologs to show different phase behaviour as a function of chain length [67]. Phase behaviour of ILCs is therefore determined by a critical balance between hydrophobic interactions of the alkyl chains, and ionic electrostatic interactions that depend on cation and anion structures, and this has been confirmed by recent molecular simulation [68-74].

*3.3 Thermal stabilities of asymmetric viologen bistriflimides (6BPn)*

The stabilities for all asymmetric viologen salts were studied by TGA analyses and are defined as the temperature (°C) at which a 5 % weight loss for each of the salts occurred at a heating rate of 10 °C/min in nitrogen. Despite the presence of flexible alkyl chains, TGA thermograms of some of these salts as shown in Fig. 6 (Fig. S26) display relatively high thermal stabilities that are in the temperature range of 331-337 °C (Table 1). These temperatures gradually decrease slightly with the increase in carbon number in the alkyl chain. Triflimide is one of best counterion that imparts the high thermal stability of any ionic liquids, ILCs and ionic polymers reported in the literature [75-77], because it has non-nucleophilic character being the conjugate base of a super acid. Therefore, it causes decomposition of the associated cationic moieties nucleophilically at relatively high temperatures.

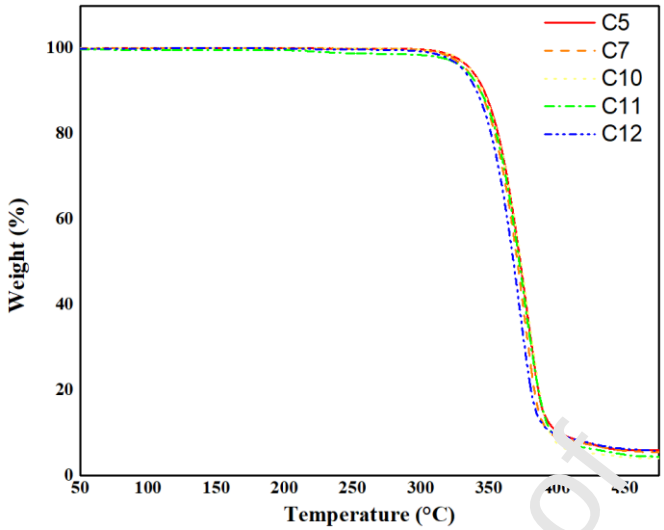


**Fig. 6** TGA thermograms of 6BP5, 6BP7, 6BP10, 6BP11 and 6BP12 obtained at a heating rate of 10 ℃ /min in nitrogen.

*3.4. Conductivity and dielectric response*

We now study the conductivity and dielectric response of selected 6BPn(s), for *n*= 14, 11, 7 and 5, and Fig. 7 and Fig. S27 show the results of 6BP14 as a function of temperature and frequency. The rest of ILCs under study exhibit comparable responses (see Fig. S28 and Fig. S29), except for 6BP5, which crystallised in the ITO cells at high temperatures, hence precluding a complete dielectric analysis on this sample. Both the dielectric elastic constant, $\varepsilon'$, and loss modulus, $\varepsilon''$, of the 6BPCn(s) depict very high values, consistent with the large polarity of ILCs. There are two main frequency regions of interest in the range under study. At sufficiently low frequencies, $\varepsilon''$ values rise to $\sim 10^3$, which can be assigned to long-range motions of ionic charges (probably the bistriflimide ions) between the electrodes. At higher frequencies, on the other hand, $\varepsilon'$ drops giving rise to well-defined peaks of the loss factor, $\varepsilon''$. The appearance of conductivity plateaus in the $\sigma'$ plots of Fig. 7 in the same frequency/temperature range, suggests that this process must be ascribed to short-range direct current conductivity, DC ($\sigma_{dc}$) in 6BP14 [78]. We note that samples with *n*=14 to 7 showed no signs of crystallisation during the dielectric

measurements, see Fig. 8 (Fig. S30), and the conductivity must be related to motions within smectic phases. The assignation of these dielectric phenomena to conductivity, rather than to polarization of functional groups, is confirmed by drops of the imaginary electrical modulus, M″, at decreasing frequencies, with slopes of around 1 in the corresponding double logarithmic plots, see Fig. S27 (c). In reference [45], some remarks on ac conduction in disordered solids are provided. We have investigated the thermal activation of the high-frequency conductivity process for 6BP14, 6BP11 and 6BP7. The dielectric loss factor peaks, $\varepsilon''$, shift to lower frequencies on cooling, see for example Fig. S27(b), confirming that this process must be ascribed to a dielectric relaxation [79]. The maxima of the $\varepsilon''$ peaks ($\varepsilon''_{max}$) were obtained and the corresponding Arrhenius plots were prepared, see Fig. 7 for 6BP14 (left axis). The temperature dependence of $\varepsilon''_{max}$ mirrors the conductivity relaxation times,$1/\tau_\sigma$, obtained from the $\sigma_{dc}$ conductivity plateaus in Fig. 7. Hence, we believe that the reorientations of the 4,4′-bipyridinium cores under the alternating electrical fields must promote charge mobility, *via* short-range ionic hoping.

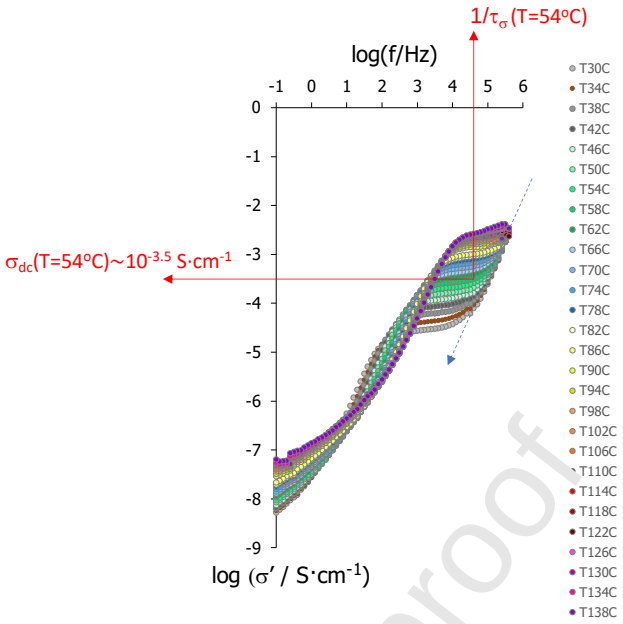


**Fig. 7**. Temperature dependence of the real component of the complex conductivity, σ′, of 6BP14,

and estimate of direct current conductivity, $\sigma_{dc}$. Dotted arrow indicates direction on cooling from the isotropic melt (T=140 °C) to room temperature (T=20 °C).

All 6BP*n* samples under study display high DC conductivities, $\sigma_{dc}$, and their maximum values are summarised in Table 2. Such high conductivities found in ionic liquid crystals (ILCs), can be associated to the small nanostructure of our viologens, with separated ionophilic regions from insulating alkyl chains [80,81]. In some precedent works by Percec and Kato, for example, sodium, phosphonium and ammonium salts of mini-dendrons reached $\sigma_{dc} \sim 10^{-6}$ to $10^{-4}$ S cm$^{-1}$ through columnar phases at room temperature [82-85]. Even though cubic phases tend to promote particularly high conductivities due to the 3D interconnectivity, lamellar LC phases promoted by rod-like molecules can also assist conductivity by reducing ionic aggregation in electrolytes [86-88]. Cherian et al.[89] have very recently reported parallel conductivities of $10^{-}$

$^{3}/10^{-2}$ S $cm^{-1}$ by surfactant complexes containing *n*-alkylamines and 1-(4-sulfobutyl)-3-methylimidazolium

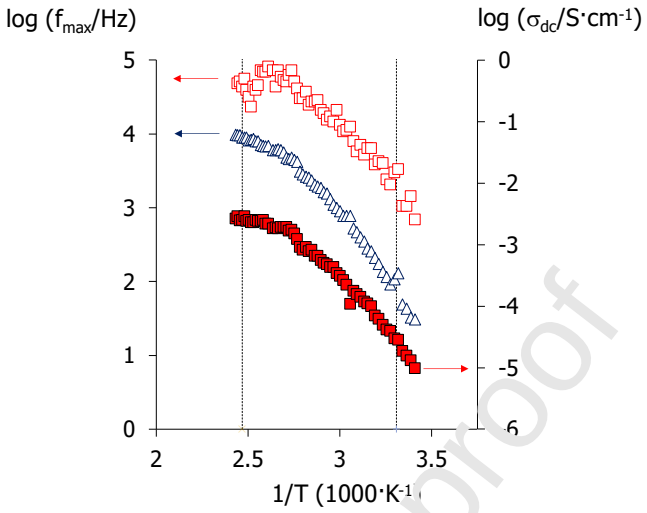


**Fig. 8.** Arrhenius plots corresponding to the thermal activation of: the dielectric relaxation at high frequencies ($\varepsilon''_{max}$, △) and DC conductivity relaxation times ($1/\tau_{\sigma}$, □) and values ($\sigma_{dc}$, ■), measured for 6BP14.

hydrogen sulfate. These values are like those shown here, and are superior to some state-of-the-art polymerized ionic liquid electrolytes [90], and comparable to phosphonium or imidazolium-based ionic liquids ($10^{-2}$ S $cm^{-1}$ at 30 °C) and to dicationic imidazolium salts forming SmA phases ($10^{-6}$ to $10^{-4}$ S $cm^{-1}$ near room temperature) [91-93].

It is widely assumed that conductivity through ionic liquid crystals depends on the molecular mobility of the ionogenic/ionophilic polar sites [94], which can be hindered in oligomers and polymers [95,96]. The large ionic conductivities exhibited by 6BP*n*(s) must result from a combination of efficient ionic solubilisation in the smectic domains and molecular mobility of the 4,4′-bipyridinium cores, which lead to highly delocalised, noncoordinating triflimide ions capable to migrate within the SmT domains, as illustrated in Fig. 9 [97]. We note, however, that Fig. 7 (as well as Fig. S27), depicts a clear Vogel-Fulcher-Tammann (VFT)

behaviour, indicating that the dielectric and conductivity response of 6BP14 (and its analogues) is strongly coupled to segmental-type motions [98,99]. Our results suggest the existence of an apparent glass transition temperature,

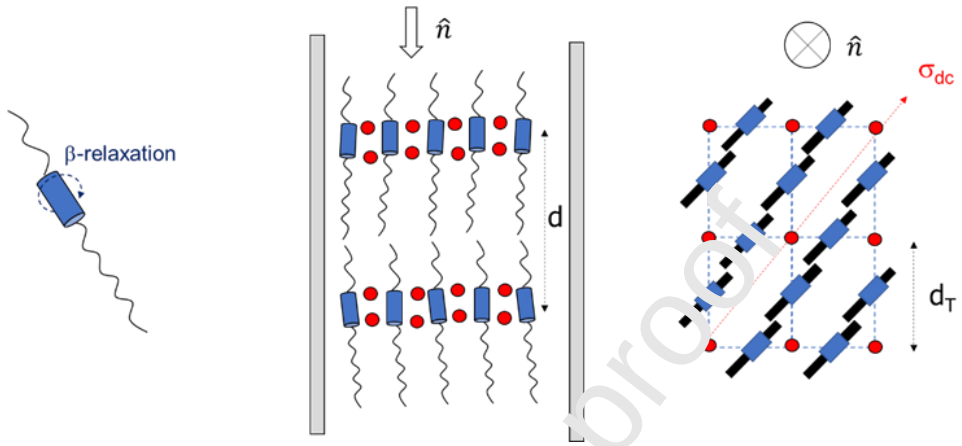


**Fig. 9.** Schematic representation of the ionic conductivity ($\sigma_{dc}$) mediated by the β-relaxation in the 6BP*n*(s), perpendicular to the smectic phase director, $\hat{n}$.

$T_g$, at which the mesogenic units start to become mobile and promote ionic conductivity. We have fitted the $\varepsilon''_{max}$ curves to VFT equations,

$$\ln\left(f_{\varepsilon''_{max}}/Hz\right) = \ln(f_0) - \frac{B}{T - T_0} \qquad \text{Eq. 4}$$

where $f_0$ is the frequency in the limit of high temperatures, $B$ is related to the activation energy of the dielectric relaxation (and therefore ionic conduction), and $T_0$ is the Vogel temperature, above which molecular motions onset. The results for different 6BP*n* samples are also summarized in Table 2. The VFT behaviour reflects on strong viscous effects, associated to the solid-like character of ILCs and the bulkiness of the triflimide ions. Even thought we could expect that longer chain lengths could hinder anion-cation iterations and conductivity [100,101], Table 2 suggests that the effect of the alkyl chains length is very limited in the 6BP*n*(s), which is

consistent with the preferential location of the ionic charges around the polar 4,4′-bipyridinium cores. These results imply that the microphase separation between polar and non-polar regions may play a major role in the conductivity of our ILCs [102], and we have calculated apparent activation energies in the smectic T phase for $\varepsilon''_{max}$ (hence $\sigma_{dc}$), considering linear temperature ranges in the Arrhenius plots. Interestingly, the $E_a^{ap}$ values calculated in this work fall within the same range (30 – 60 KJ $mol^{-1}$) as those described for the so-called β relaxation in azobenzene-based liquid crystals, associated to the rotation of the mesogenic core [103-107]. Whereas low-ordered SmA phases with planar alignments can result in ionic domains being perpendicularly aligned respect to the smectic phase director, $\hat{n}$, the relative tilt of the layers in the SmT phase of our asymmetric ILCs may affect ionic conductivity. We have applied increasing alternating electrical fields through the 6BP14 sample at different temperatures, to realign the phase director, and we have observed that the capacitance maxima are reached in the interval $V_{max} \sim 2$ to 12 $V_{rms}$, but not for the maximum voltage (20 $V_{rms}$), see Fig. S26. We hypothesise that these $V_{max}$ values may correspond to the orientation when the ionic channels in Fig. 9 are aligned perpendicularly to the electrodes, hence minimising conductivity "tortuosity". As expected, the dependence of $V_{max}$ with temperature seen in Fig. S31(b), correlates well with $T_m$, as a crossover of the trends in the smectic and crystal phases. The effect of realignment of SmT domains *via* AC fields will be further investigated in a follow up study.

**Table 2.** Thermal activation parameters obtained from the high-frequency dielectric relaxation ($\varepsilon''_{max}$) and DC conductivity ($\sigma_{dc}$): Vogel-Fulcher-Tammann (VFT) parameters and apparent activation energy, $E_a^{ap}$, in the pseudo-linear smectic ranges.

| Sample ID | VTF behaviour ($\varepsilon''_{max}$) | Conductivity ($s_{dc}$) |
|---|---|---|

| | $\ln(f_0/Hz)$ | B / K | $T_0$/ K | -log($\sigma_{dc\_max}$ / S cm$^{-1}$) | $E_a^{ap}$ / kJ mol$^{-1}$* |
|---|---|---|---|---|---|
| 6BP14 | 11.94 | 422.9 | 251.5 | 2.43 | 54.4 |
| 6BP11 | 10.51 | 226.6 | 252.6 | 2.54 | 35.27 |
| 6BP7 | 10.49 | 182.8 | 250.0 | 2.55 | 49.42 |

## 4. Conclusions

We have synthesized and characterised a series of asymmetric viologen bis(triflimide) salts that contain short (C6) and long (C*n*, $5 \leq n \leq 20$) alkyl chains (6BPn). Their thermotropic LC properties were determined by DSC, POM and VT-XRD, showing crystal to SmT phase transitions, $T_m$s, at temperatures as low as -12 °C, and relatively high clearing temperatures, $T_i$s. Their large LC ranges, ordered structures and excellent thermal stabilities below ~330 °C, makes them suitable for many potential applications, including catalysts in organic reactions with high yields and selectivities. These ILCs exhibit high ionic conductivity through their SmT phases, in the range of $10^{-2.5}$ S cm$^{-1}$ . The overlapping between polar regions, consisting of stacks of 4,4′-bipyridinium units, seems to be a prerequisite to yield ionic conductivity. The highly-ordered SmT template requires cooperative motions of the rod-like molecules that lead to VFT behaviour [101,102]. These motions are activated at low temperatures, and the high conductivities confirm the potential of the 6BP*n*(s) to be used as smectic glasses in several applications.

## Author contributions

Pradip K. Bhowmik, Michael R. Fisch and Alfonso Martinez-Felipe: Conceptualization; Pradip K. Bhowmik, Michael R. Fisch and Alfonso Martinez-Felipe: Data curation; Pradip K. Bhowmik, Michael R. Fisch and Alfonso Martinez-Felipe: Formal analysis; Pradip K. Bhowmik,

Michael R. Fisch and Alfonso Martinez-Felipe: Funding acquisition; Omar Noori, Si L. Chen, Haesook Han, Christina M. Robb, and Aaron Variyam: Investigation; Omar Noori, Si L. Chen, Haesook Han, Christina M. Robb, and Aaron Variyam: Methodology; Pradip K. Bhowmik, Michael R. Fisch and Alfonso Martinez-Felipe: Project administration; Pradip K. Bhowmik, Michael R. Fisch and Alfonso Martinez-Felipe: Resources; Pradip K. Bhowmik, Michael R. Fisch and Alfonso Martinez-Felipe: Software; Pradip K. Bhowmik, Michael R. Fisch and Alfonso Martinez-Felipe: Supervision; Pradip K. Bhowmik, Michael R. Fisch and Alfonso Martinez-Felipe: Validation; Pradip K. Bhowmik, Michael R. Fisch and Alfonso Martinez-Felipe: Visualization; Pradip K. Bhowmik, Michael R. Fisch and Alfonso Martinez-Felipe: Roles/Writing - original draft; Writing - re Pradip K. Bhowmik, Michael R. Fisch and Alfonso Martinez-Felipe: view & editing.

**Declaration of competing interest**

The authors declare that they have no known competing financial interests or personal relationships that could have appeared to influence the work reported in this paper.

**Acknowledgments**

This research is in part supported by the NSF EPSCoR RING-TRUE III grant no. 0447416, NSF-SBIR grant no. OII-0610753, NSF-STTR grant no. IIP-0740289 and NASA GRC contract no. NNX10CD25P (PKB). We thank Ronald C. G. Principe for making the Figures and Tables for this article. Acknowledgment is made to the donors of the American Chemical Society Petroleum Research Fund grant no. 59345-ND7 for partial support of this research by CMR and MRF. AMF would like to thank the Carnegie Trust for the Universities of Scotland, for the Research Incentive Grant RIG008586, the Royal Society and Specac Ltd., for the

Research Grant RGS\R1\201397, and the Royal Society of Chemistry for the award of a mobility grant (M19-0000).

**References**

[1] P.M.S. Monk, The Viologens Physicochemical Properties, Synthesis and Applications of the Salts of 4,4-Bipyridine, Wiley, New York, 1998, pp 1-311.

[2] L. Striepe, T. Baumgartner, Viologens and Their Application as Functional Materials, Chem. Eup. J. 23, (2017) 16924-16940.

[3] C.R. Rigby, H. Han, P.K. Bhowmik, M. Bahari, A. Chang, J.N. Harb, R.S. Lewis, G.D. Watt, Soluble Viologen Polymers as Carbodydrate Oxidation Catalysts for Alkaline Fuel Cells, J. Electroanal. Chem. 823 (2018) 416-421.

[4] J. Ding, C. Zheng, L. Wang, C. Lu, B. Zhang, Y. Chen, M. Li, G. Zhai, X. Zhuang, Viologen-inspired functional materials: synthetic strategies and applications, J. Mater. Chem. A 7 (2019) 23337-23360.

[5] T. Hatazawa, R.H. Terrill, R.W. Murray, Microelectrode Voltammetry and Electron Transport in an Undiluted Room Temperature Melt of an Oligo(ethylene glycol)-Tailed Viologen, Anal. Chem. 68 (1996) 597-603.

[6] K. Ito-Akita, H. Ohno, Low Temperature Molten Viologens-Phase Transitions and Electrochemical Properties, Electrochem. Soc. Procced. 99-14 (1999) 193-201.

[7] V. Causin, G. Saielli, Effect of a structural modification of the bipyridinium core on the phase

behaviour of viologen-based bistriflimide salts, J. Mol. Liq. 145 (2009) 41–47.

[8] V. Causin, G. Saielli, Effect of asymmetric substitution on the mesomorphic behaviour of low-

melting viologen salts of bis(trifluoromethanesulfonyl)amide, J. Mater. Chem. 19 (2009) 9153–9162.

[9] M. Bonchio, M. Carraro, G. Casella, V. Causin, F. Rastrelli, G. Saielli, Thermal behaviour and electrochemical properties of bis(trifluoromethanesulfonyl)amide and dodecatungstosilicate viologen dimers, Phys. Chem. Chem. Phys. 14 (2012) 2710– 2717.

[10] H.Q.N. Gunaratne, P. Nockemann, S. Olejarz, S. M. Reid, K.R. Seddon, G. Srinivasan, Ionic Liquids with Solvatochromic and Charge-Transfer Functionalities Incorporating the Viologen Moiety, Aust. J. Chem. 66 (2013) 607-611.

[11] N. Jordäo, L. Cabrita, F. Pina, L.C. Branco, Novel Bipyridinium Ionic Liquids as Liquid Electrochromic Devices, Chem. Eur. J. 20 (2014) 3982-3988.

[12] H. Tahara, Y. Furue, C. Suenaga, C. Sagara, A Dialkyl Viologen Ionic Liquid: X-ray Crystal Structure Analysis of Bis(trifluoromethanesulfonyl)imide Salts, Cryst. Growth Des. 15 (2015) 4735-4740.

[13] N. Jordäo, H. Cruz, A. Branco, F. Pina, L.C Branco, Electrochromic Devices Based on Disubstituted Oxo-Bipyridinium Ionic Liquids, ChemPlusChem. 80 (2015) 202-208.

[14] L.P. Yu, E.T. Samulski, Ionomeric Liquid Crystals, in: Oriented Fluids and Liquid Crystals, A.C. Griffin, J.F. Johnson, (Eds), Plenum, New York, 1984, Vol. 4, pp 697-704.

[15] I. Tabushi, K. Yamamura, K. Kominami, Electric Stimulus-Response Behavior of Liquid-Crystalline Viologen, J. Am. Chem. Soc. 108 (1986) 6409-6410.

[16] K. Yamamura, Y. Okada, S. Ono, K. Kominami, I. Tabushi, New Liquid Crystalline Viologens Exhibiting Electric Stimulus-Response Behavior, Tetrahedron Lett. 28 (1987)

6475-6478.

[17] Y. Haramoto, M. Yin, Y. Matukawa, S. Ujiie, M. Nanasawa, A new ionic liquid crystal compound with viologen group in the principal structure, Liq. Cryst. 19 (1995) 319-320.

[18] P.K. Bhowmik, H. Han, J.J. Cebe, R.A. Burchett, A. Acharya, S. Kumar, Ambient temperature thermotropic liquid crystalline viologen bis(triflimide) salts, Liq. Cryst. 30 (2003) 1433–1440.

[19] P.K. Bhowmik, H. Han, I.K. Nedeltchev, J.J. Cebe, Room-Temperature Thermotropic Ionic Liquid Crystals: Viologen Bis(triflimide) Salts, Mol. Cryst. Liq. Cryst. 419 (2004) 27-46.

[20] P.K. Bhowmik, S.T. Killarney, J.R.A. Li, J.J. Koh, H. Han, L. Sharpnack, D.M. Agra-Kooijman, M.R. Fisch, S. Kumar, Thermotropic liquid-crystalline properties of extended viologen bis(triflimide) salts, Liq. Cryst. 45 (2018) 872-885.

[21] G. Casella, V. Causin, F. Rastrelli, G. Saielli, Viologen-based ionic liquid crystals: induction

of a smectic A phase by dimerisation, Phys. Chem. Chem. Phys. 16 (2014) 5048– 5051.

[22] G. Casella, V. Causin, F. Rastrelli, G. Saielli, Ionic liquid crystals based on viologen dimers:

tuning the mesomorphism by varying the conformational freedom of the ionic layer, Liq. Cryst. 43 (2016) 1161-1173.

[23] K. Tanabe, T. Yasuda, M. Yoshio, T. Kato, Viologen-Based Redox-Active Ionic Liquid Crystals Forming Columnar Phases, Org. Lett. 9 (2007) 4271-4274.

[24] S. Asaftei, M. Ciobanu, A.M. Lepadatu, E. Song, U. Beginn, Thermotropic ionic liquid crystals by molecular assembly and ion pairing of 4,4′-bipyridinium derivatives and tris(dodecyloxy)benzenesulfonates in a non-polar solvent, J. Mater. Chem. 22 (2012)

14426-14437.

[25] R.T. Wang, G.-H. Lee, C.K. Lai, Anion-induced ionic liquid crystals of diphenylviologens, J. Mater. Sci. C 6 (2018) 9430-9444.

[26] K. Binnemans, Ionic Liquid Crystals, Chem. Rev. 105 (2005) 4148-4204.

[27] L. Douce, J.-M. Suisse, D. Guillon, A. Taubert, Imidazolium-based liquid crystals: a modular platform for versatile new materials with finely tuneable properties and behaviour, Liq. Cryst. 38 (2011) 1653-1661.

[28] K. Axenov, S. Laschat, Thermotropic ionic liquid crystals, Materials 4 (2011) 206-249.

[29] V. Causin, G. Saielli, Ionic liquid crystals, in Green Solvents II. Properties and Applications of Ionic Liquids, A. Mohammad, D. Inamuddin (Eds.), Springer, London, UK, 2012, pp 79-118.

[30] M. Mansueto, S. Laschat, Ionic Liquid Crystals, in Handbook of Liquid Crystals, Vol. 6: Nanostructured and Amphiphilic Liquid Crystals, 2nd ed., J.W. Goodby, P.J. Collings, T. Kato, C. Tschierske, H. Gleeson, P. Raynes (Eds.), Wiley-VCH, Weinheim, Germany, 2014, pp 231-280.

[31] J. Sakuda, E. Hosono, M. Yoshio, T. Ichikawa, T. Matsumoto, H. Ohno, H. Zhou, T. Kato, Liquid-Crystalline Electrolytes for Lithium-Ion Batteries: Ordered Assemblies of a Mesogen-Containing Carbonate and a Lithium Salt, Adv. Funct. Mater. 25 (2015) 1206-1212.

[32] K. Goossens, K. Lava, C.W. Bielawski, K. Binnemans, Ionic Liquid Crystals: Versatile Materials, Chem. Rev. 116 (2016) 4643-4807.

[33] A.A. Fernandez, P.H.J. Kouwer, Key Developments in Ionic Liquid Crystals, Int. J. Mol. Sci. 17 (2016) 731.

[34] D. Högberg, B. Soberats, R. Yatagai, S. Uchida, M. Yoshio, L. Kloo, H. Segawa, T. Kato, Liquid-Crystalline Dye-Sensitized Solar Cells: Design of Two-Dimensional Molecular Assemblies for Efficient Ion Transport and Thermal Stability, Chem. Mater. 28 (2016) 6493-6500.

[35] T. Kato, M. Ypshio, T. Ichikawa, B. Soberats, H. Ohno, M. Funahashi, Transport of ions and electrons in nanostructured liquid crystals, Nat. Rev. Mater. 2 (2017) 17001.

[36] M.J. Pastor, I. Sánchez, J.A. Campo, R. Schmidt, M. Cano, New Pyrazolium Salts as a Support for Ionic Liquid Crystals and Ionic Conductors, Materials 11 (2018) 548.

[37] Y. Song, X. Tang, S. Kong, L. Bai, X. He, F. Meng, Synthesis and characterization of hexamethylenetetramine-based ionic liquid crystals, J. Mol. Struc. 178, (2019) 135-141.

[38] Hyunho Chae, Y.-H. Lee, M. Yang, W.-J. Yoon, D.K. Yoon, K.-U. Jeong, Y.H. Song, U.H. Choi, M. Lee, Interesting phase behaviors and ion-conducting properties of dicationic N-alkylimidazolium tetrafluoroborate salts, RSC Adv. 9 (2019) 3972-3978.

[39] T. Ichikawa, T. Kato, H. Ohno, Dimension control of ionic liquids, Chem. Commun. 55 (2019) 8205-8214.

[40] F. Yuan, S. Chi, S. Deng, Y. Zou, S. Lv, L. Bao, J. Wang, Ionic liquid crystal with fast ion-conductive tunnels for potential application in solvent-free Li-ion batteries, Electrochimica Acta 294 (2019) 249-259.

[41] X. Wang, M. Sternberg, F.T.U. Kohler, B.U. Melcher, P. Wasserscheid, K. Meyer, Long-alkyl-chain-derivatized imidazolium salts and ionic liquid crystals with tailor-made properties, RSC Adv. 4 (2014) 12474-12481.

[42] T. D. Do, A.R. Schmitzer, Intramolecular Diels Alder reactions in highly organized imidazolium salt-based ionic liquid crystals, RSC Adv. 5 (2015) 636-639.

[43] D.T. Do, A.R. Schmitzer, Highly Ordered Rectangular Columnar Ionic Liquid Crystals: A More Efficient Medium for Intramolecular Diels Alder Reactions, ChemistrySelect 1 (2016) 2448-2453.

[44] D.W. Bruce, Y. Gao, J.N.C. Lopes, K. Shimizu, John M. Slattery, Liquid-Crystalline Ionic Liquids as Ordered Reaction Media for the Diels–Alder Reaction, Chem. Eur. J. 22 (2016) 16113-16123.

[45] J.C. Dyre, Some remarks on ac conduction in disordered solids, J. Non-Cryst. Solid 135 (1991) 219-216.

[46] I. Hodge, M. Ingram, A. West, New Methods for analyzing ac behavior of polycrystalline solid electrolytes, J. Electroanal. Chem. 58 (1975) 429-432.

[47] G.W. Gray, J.W.G. Goodby, Smectic Liquid Crystals: Textures and Structures, Leonard Hill, Glasgow, 1984.

[48] P.J. Collins, M. Hird, Introduction to Liquid Crystals Chemistry and Physics, Taylor & Francis, Bristol, PA, 1997.

[49] Handbook of Liquid Crystals, vols. 1-3, D. Demus, J.W. Goodby, G.W. Gray, H.-W. Spiess, V. Vill (Eds.), Wiley-VCH, Weinheim, Germany, 1998.

[50] I. Dierking, Textures of Liquid Crystals, Wiley-VCH, Weinheim, Germany, 2003.

[51] Handbook of Liquid Crystals: 8 Volume Set, 2nd edition, J.W. Goodby, P.J. Collings, T. Kato, C. Tschierske, H.F. Gleeson, P. Raynes (Eds), Wiley-VCH, Weinheim, Germany, 2014.

[52] J. Golding, S. Forsyth, D.R. MacFarlane, M. Forsyth, G.B. Deacon, Methanesulfonate and p-toluenesulfonate salts of the N-methyl-N-alkylpyrrolidinium and quaternary ammonium cations: novel low cost ionic liquids, Green Chem. 4 (2002) 223-229.

[53] J. De Roche, C.M. Gordon, C.T. Imrie, M.D. Ingram, A.R. Kennedy, F. Lo Celso, A. Triolo, Application of complementary experimental techniques to characterization of the phase behavior of [$C_{16}$mim][$PF_6$] and [$C_{14}$mim][$PF_6$], Chem. Mater. 15 (2003) 3089-3097.

[54] P.K. Bhowmik, H. Han, I.K. Nedeltchev, J.J. Cebe, S.W. Kang, S. Kumar, Synthesis and characterization of ionic liquids: viologen bis{tetrakis[3,5-bis(trifluoromethyl)phenyl]borate} salts, Liq. Cryst. 33 (2006) 891-906.

[55] T.J. Jo, W.L. McCurdy, O. Tanthmanatham, T.K. Kim, H. Han, P.K. Bhowmik, B. Heinrich, B. Donnio, Synthesis and characterization of luminescent tricationic salts of mesitylene and stilbazolium moieties, J. Mol. Struc. 1019 (2012) 174-182.

[56] P.K. Bhowmik, C.I. Lee, J.J. Koh, H. Han, A. Jubair, V. Kartazaev, S.K. Gayen, Synthesis, optical, and thermal properties of 2,4,6-tris(4-substituted phenyl)pyrylium tosylates and triflimides, J. Mol. Struc. 1202 (2020) 127325.

[57] C.M. Gordon, J.D. Holbrey, A.R. Kennedy, K.R. Seddon, Ionic liquid crystals: hexafluorophosphate salts, J. Mater. Chem. 8 (1998) 2627-2636.

[58] J.D. Holbrey, K.R. Seddon, The phase behaviour of 1-alkyl-3-methylimidazolium tetrafluoroborates; ionic liquids and ionic liquid crystals, J. Chem. Soc. Dalton Trans. (1999) 2133-2139.

[59] M. Arkas, D. Tsiourvas, C.M. Paleos, A. Skoulios, Smectic Mesophases from Dihydroxy Derivatives of Quaternary Alkylammonium Salts, Chem. Eur. J. (1999) 3202-3207.

[60] K. Ohta, T. Sugiyama, T. Nogami, A smectic T phase of 1,4-dialkyl-1,4-diazoniabicyclo[2.2.2]octane dibromides, J. Mater. Chem. 10 (2000) 613-616.

[61] K. Goossens, K. Lava, P. Nockemann, K. Van Hecke, L. Van Meervelt, K. Driesen, C. Görller-Walrand, K. Binnemans, T. Cardinaels, Pyrrolidinium Ionic Liquid Crystals, Chem.

Eur. J. 15 (2009) 656-674.

[62] M. Zhou, J. Zhang, S. Wang, D. Boyer, H. Guo, W. Li, L. Wu, Laterally substituted ionic liquid crystals and the resulting rheological behavior, Soft Matter 8 (2012) 7945-7951.

[63] M. Yang, K. Stappert, A.-V. Mudring, Bis-cataionic ionic liquid crystals, J. Mater. Chem. C 2 (2014) 458-473.

[64] P.K. Bhowmik, A. Chang, J. Kim, E. J. Dizon, R.C.G. Principe, H. Han, Thermotropic Liquid-Crystalline Properties of Viologens Containing 4-n-alkylbenzenesulfonates, Crystals 9 (2019) 77.

[65] P.K. Bhowmik, M.K.M. Al-Karawi, S.T. Killarney, E.J. Dizon, A. Chang, J. Kim, S.L. Chen, R.C.G. Principe, A. Ho, H. Han, H.D. Mandal, R.G. Cortez, B. Gutierrez, K. Mendez, L. Sharpnack, D.M. Agra-Kooijman, M.R. Fisch, S. Kumar, Thermotropic Liquid-Crystalline and Light-Emitting Properties of Bis(4-alkoxyphenyl) Viologen Bis(triflimide) Salts, Molecules 25 (2020) 2435.

[66] M. Arkas, I. Kitsou, F. Petraki, Mimicking the behaviour of rigid rod molecules. Smectic H liquid crystals from amphiphilic quaternary ammonium salts, Liq. Cryst. 45 (2018) 70-83.

[67] A. Kumar, A.K. Srivastava, S.N. Tiwari, N. Masra, D. Sharma, Evolution of Anisotropy, First Order Hyperpolarizability and Electronic Parameters in p-Alkyl-p′-Cyanobiphenyl Series of Liquid Crystals: Odd-Even Effect Revisited, Mol. Cryst. Liq. Cryst. 681 (2019) 23-31.

[68] Y. Ji, R. Shi, Y. Wang, G. Saielli, Effect of the Chain Length on the Structure of Ionic Liquids: From Spatial Heterogeneity to Ionic Liquid Crystals, J. Phys. Chem. B 117 (2013) 1104-1109.

[69] G. Saielli, G.A. Voth, Y. Wang, Diffusion mechanisms in smectic ionic liquid crystals:

Insights from coarse-grained MD simulations, Soft Matter 9 (2013) 5716-5725.

[70] Y.V. Nelyubina, A.S. Shaplov, E.I. Lozinskaya, M.I. Buzin, Y.S. Vygodskii, A New Volume-Based Approach for Predicting Thermophysical Behavior of Ionic Liquids and Ionic Liquid Crystals, J. Am. Chem. Soc. 138 (2016) 10076-10079.

[71] M.A.R. Martins, P.J. Carvalho, D. Alves, C. Dariva, M.C. Costa, R.A.S. Ferreira, P.S. Andre´, P. Morgado, S.P. Pinho, E.J. M. Filipe, J.A.P. Coutinho, Surface crystallization of ionic liquid crystals, Phys. Chem. Chem. Phys. 21 (2019) 17792-17800.

[72] G. Saielli, K. Satoh, A coarse-grained model of ionic liquid crystals: the effect of stoichiometry on the stability of the ionic nematic phase, Phys. Chem. Chem. Phys. 21 (2019) 20327-20337.

[73] G. Saielli, Comparison of the Ionic Liquid Crystal Phase of $[C_{12}C_1im][BF_4]$ and $[C_{12}C_1im]Cl$ by Atomistic MD Simulations, Crystals 10 (2020) 253.

[74] W. Cao, B. Senthilkumar, V. Causin, V. P. Swamy, Y. Wang, G. Saielli, Influence of the ion size on the stability of the smectic phase of ionic liquid crystals, Soft Matter 16 (2020) 411-420.

[75] A.K. Nedeltchev, H. Han, P.K. Bhowmik, Design and synthesis of photoactive ionic amorphous molecular materials, J. Mater. Chem. 21 (2011) 12717-12724.

[76] T.S. Jo, A.K. Nedeltchev, B. Biswas, H. Han, P.K. Bhowmik, Synthesis and characterization of poly(pyridinium salt)s derived from various aromatic diamines, Polymer 53 (2012) 1063-1071.

[77] T.S. Jo, J.J. Koh, H. Han, P.K. Bhowmik, Solution, thermal and optical properties of bis(pyridinium salt)s as ionic liquids, Mater. Chem. Physics 139 (2013) 901-910.

[78] A.W. Brown, A. Martinez-Felipe, Ionic conductivity mediated by hydrogen bonding in

liquid crystalline 4-n-alkoxybenzoic acids, J. Mol. Struc. 1197 (2019) 487-496.

[79] Z. Wojnarowska, J. Knapik, M. Diaz, A. Ortiz, I. Ortiz, M. Paluch, Macromolecules 47 (2014) 4056-4065.

[80] C.H. Chan, H. Kammer, Impedance spectra of polymer electrolytes, Ionics 23 (2017) 2327-2337.

[81] B. Cho, Nanostructured organic electrolytes, RSC Adv. 4 (2014) 395-405.

[82] V. Percec, G. Johansson, J. Heck, G. Ungar, S.V. Batty, Molecular Recognition Directed Self -assembly of Supramolecular Cylindrical Channel-like Architectures from 6,7,9,10,12,13,15,16-Octahydro-l,4,7,1 O,l3- pentaoxabenzocyclopentadecen-2-ylmethyl 3,4,5-Tris(p-dodecyloxybenzyloxy) benzoate, J. Chem. Soc. Perkin Trans. 1 (1993) 1411-1420.

[83] M. Yoshio, T. Mukai, H. Ohno, T. Kato, One-dimensional ion transport in self-organized columnar ionic liquids, J. Am. Chem. Soc. 126 (2004) 994-995.

[84] M. Yoshio, T. Ichikawa, H. Shimura, T. Kagata, A. Hamasaki, T. Mukai, H. Ohno, T. Kato, Columnar liquid-crystalline imidazolium salts. Effects of anions and cations on the mesomorphic properties and ionic conductivity, Bull. Chem. Soc. Jpn. 80 (2007) 1836-1841.

[85] S. Yazaki, Y. Kamikawa, M. Yoshio, A. Hamasaki, T. Mukai, H. Ohno, T. Kato, Ionic liquid crystals: Self-assembly of imidazolium salts containing an L-glutamic acid moiety, Chem. Lett. 37 (2008) 538-539.

[86] B. Soberats, E. Uchida, M. Yoshio, J. Kagimoto, H. Ohno, T. Kato, Macroscopic photocontrol of ion-transporting pathways of a nanostructured imidazolium-based photoresponsive liquid crystal, J. Am. Chem. Soc. 136 (2014) 9552-9555.

[87] J. Liu, Y. Zheng, Y. Liao, X. Zheng, G. Ungar, P. Wright, Organisation in two series of

low-dimensional polymer electrolytes with high ambient lithium salt conductivity, Faraday Discuss. 128 (2005) 363-378.

[88] S.M. Alauddin, N.F.K. Aripin, T.S. Velayutham, A. Martinez-Felipe, Liquid Crystalline Copolymers Containing Sulfonic and Light-Responsive Groups: From Molecular Design to Conductivity, Molecules 25 (2020) 2579.

[89] T. Cherian, D.R. Nunes, T.G. Dane, J. Jacquemin, U. Vainio, T.T.T. Myllymäki, J.V.I. Timonen, N. Houbenov, M. Maréchal, P. Rannou, O. Ikkala, Supramolecular Self-Assembly of Nanoconfined Ionic Liquids for Fast Anisotropic Ion Transport, Adv. Funct. Mater. 29 (2019) 1905054.

[90] A. Jourdain, A. Serghei, E. Drockenmuller, Enhanced Ionic Conductivity of a 1,2,3-Triazolium-Based Poly(siloxane ionic liquid) Homopolymer, ACS Macro Lett. 5 (2016) 1283-1286.

[91] A. Serghei, M. Samet, G. Boiteux, A. Kellel, Dielectric properties of ionic liquids at metal interfaces: Electrode polarization, characteristic frequencies, scaling laws, in: Dielectric Properties of Ionic Liquids, M. Paluch (Ed.), Springer, Switzerland, 2016.

[92] D.M. Maximean, V. Cîrcu, C.P. Ganea, Dielectric properties of a bisimidazolium salt with dodecyl sulfate anion doped with carbon nanotubes, Beilstein J. Nanotechnol. 9 (2018) 164-174.

[93] C.P. Ganea, V. Cîrcu, D.M. Maximean, Effect of titanium oxide nanoparticles on the dielectric properties and ionic conductivity of a new smectic bis-imidazolium salt with dodecyl sulfate anion and cyanobiphenyl mesogenic groups, J. Mol. Liq. 317 (2020) 113939.

[94] K. Kishimoto, T. Suzawa, T. Yokata, T. Mukai, H. Ohno, T. Kato, Nano-segregated

polymeric film exhibiting high ionic conductivities, J. Am. Chem. Soc. 127 (2005) 15618-15623.

[95] A. Concellón, S. Hernández-Ainsa, J. Barberá, P. Romero, J. Luis Serrano, M. Marcos, Proton conductive ionic liquid crystalline poly(ethyleneimine) polymers functionalized with oxadiazole, RSC Adv. 8 (2018) 37700-37706.

[96] S. Liang, M.V. O'Reilly, U.H. Choi, H. Shiau, J. Bartels, Q. Chen, J. Runt, K.I. Winey, R.H. Colby, High Ion Content Siloxane Phosphonium Ionomers with Very Low $T_g$, Macromolecules 47 (2014) 4428-4437.

[97] C.M. Evans, C.R. Bridges, G.E. Sanoja, J. Bartels, Rachel A. Segalman, Role of Tethered Ion Placement on Polymerized Ionic Liquid Structure and Conductivity: Pendant versus Backbone Charge Placement, ACS Macro Lett. 5 (2016) 925-930.

[98] G. Fulcher, Analysis of recent measurements of the viscosity of glasses-reprint, J. Am. Ceram. Soc. 75 (1992) 1043-1059.

[99] H. Vogel, The temperature dependence law of the viscosity of fluids, Physikalische Zeitschrift, 22 (1921) 645-646.

[100] F. Xu, K. Matsumoto, R. Hagiwara, Effects of alkyl chain length on properties of 1-alkyl-methylimidazolium fluorohydrogenate ionic liquid crystals, Chem. Eur. J. 16 (2010) 12970-12976.

[101] F. Xu, K. Matsumoto, R. Hagiwara, Phase Behavior of 1-Dodecyl-3-methylimidazolium Fluorohydrogenate Salts ($C_{12}$MIm(FH)nF, n = 1.0−2.3) and Their Anisotropic Ionic Conductivity as Ionic Liquid Crystal Electrolytes, J. Phys. Chem. B 116 (2012) 10106-10112.

[102] Q. Yu, Z. Zhao, S. Tan, Preparation and proton conductivity in liquid crystals containing

sulfonic acid moiety, Emerging Materials Research 7 (2018) 218-222.

[103] A. Martinez-Felipe, L. Santonja-Blasco, J.D. Badia, C.T. Imrie, A. Ribes-Greus, Characterization of functionalized side-chain liquid crystal methacrylates containing nonmesogenic units by dielectric spectroscopy, Ind. Eng. Chem. Res. 52 (2013) 8722-8731.

[104] L. Vanti, S. Mohd Alauddin, D. Zaton, N.F.K. Aripin, M. Giacinti-Baschetti, C.T. Imrie, A. Ribes-Greus, A. Martinez-Felipe, Ionically conducting and photoresponsive liquid crystalline terpolymers: Towards multifunctional polymer electrolytes, Eur. Polym. J. 109 (2018) 124-132.

[105] S.M. Alauddin, N.F.K. Aripin, T.S. Velayutham, I. Chaganava, A. Martinez-Felipe, The role of conductivity and molecular mobility on the photoanisotropic response of a new azo-polymer containing sulfonic groups, J. Photochem. Photobiol. A: Chem. 389 (2020) 112268.

[106] R. Zentel, G. Strobl, H. Ringsdorf, Dielectric-relaxation of liquid-crystalline polyacrylates and polymethacrylates, Macromolecules 18 (1985) 960-965.

[107] A. Schonhals, D. Wolff, J. Springer, Influence of the mesophase structure on the beta-relaxation in comb-like polymethacrylates, Macromolecules 28 (1995) 6254-6257.

All authors have equally contributed to the elaboration of this paper and have equal relevant credit roles.

## Research Highlights

- Synthesis of asymmetric viologen bistriflimide salts were performed by metathesis reaction
- Their thermotropic liquid-crystalline properties were determined by experimental techniques
- They transformed into highly-ordered smectic T phases at relatively low temperatures
- They showed liquid-crystallinity in a broad range of temperatures
- Their ionic conductivity was measured and found to be in the $10^{-2.43}$ S $cm^{-1}$ range

**Declaration of competing interest**

The authors declare that they have no known competing financial interests or personal relationships that could have appeared to influence the work reported in this paper.